CHIN. PHYS. LETT. Vol. 38, No. 2 (2021) 027201

Topological-Defect-Induced Superstructures on Graphite Surface

Zi-Lin Ruan(阮子林), Zhen-Liang Hao(郝振亮), Hui Zhang(张辉), Shi-Jie Sun(孙诗杰), Yong Zhang(张永), Wei Xiong(熊玮), Xing-Yue Wang(王兴悦), Jian-Chen Lu(卢建臣)*, and Jin-Ming Cai(蔡金明)

Faculty of Materials Science and Engineering, Kunming University of Science and Technology, Kunming 650000, China

(Received 27 August 2020; accepted 18 November 2020; published online 27 January 2021)

Topological defects in graphene induce structural and electronic modulations. Knowing exact nature of broken-symmetry states around the individual atomic defects of graphene is very important for understanding the electronic properties of this material. We investigate structural dependence on localized electronic states in the vicinity of topological defects on a highly oriented pyrolytic graphite (HOPG) surface, using scanning tunneling microscopy and spectroscopy. Several inherent topological defects on the HOPG surface and the local density of states surrounding them are explored, visualized as scattering wave-related $(\sqrt{3}\times\sqrt{3})$ R30° superstructures and honeycomb superstructures. In addition, the superstructures observed near the grain boundary have a much higher decay length at specific sites than that reported previously, indicating far greater electron scattering on the quasi-periodic grain boundary.

DOI: 10.1088/0256-307X/38/2/027201

Topological defects such as vacancy dislocations and grain boundaries (GBs) are inherent in many crystalline materials. The presence of topological defects may break the perfect lattice symmetry, resulting in many novel properties. For instance, the formed defects in graphene can break the symmetry of the two-dimensional honeycomb lattice, opening up a whole research area in terms of investigating the effect of defects on the mechanical, electrical, chemical and optical properties of graphene.[1–8] Previous studies have revealed the precise structures and electronic states induced by topological defects in graphite, via a combination of scanning tunneling microscopy/spectroscopy (STM/S) experiments and theoretical calculations. In this work, with respect to novel defects observed in graphite, we also note that new electronic states are introduced in association with these defects.[9–16] Using STM/S, we observe a coexistence of $(\sqrt{3}\times\sqrt{3})$ R30° and honeycomb superstructures close to the topological defects, which have already been reported as intrinsic electronic properties of the armchair step edge of the graphite surface.[10,17]

Owing to the modified local electronic states compared to the bulk area on the graphite, topological defects can be easily distinguished using STM. In our experiment, freshly cleaved highly oriented pyrolytic graphite (HOPG), with a lower degree of crystallinity, was used to identify different defects. Figure S1 in the Supporting Information shows four typical topological defects observed during STM scanning, which manifest as distinctive bright contrasts in STM topographies, indicating a high local density of state (LDOS) in the region of the defects. In addition to the high LDOS in the center and vicinity of the defects, we also observed superstructures near the defects, i.e., $(\sqrt{3}\times\sqrt{3})$ R30° and honeycomb superstructures, extending to several nanometers around the defect, as shown in Fig. 1. The $(\sqrt{3}\times\sqrt{3})$ R30° superstructure results from the electron wave scattering of intervalley K–K' ($q = 2k_{\rm F}$, where $k_{\rm F}$ is the Fermi wave vector) occurring near the defects or armchair edges. For graphite, the Fermi wave vector is located at the corner of the Brillouin zone.[18] Therefore, the modulation of LDOS associated with the scattering wave vector q is commensurate with the underlying atomic lattice, and consequently gives rise to the $(\sqrt{3}\times\sqrt{3})$ R30° superstructure.[17] In Fig. 1(a), different STM contrast regions are separated by white dashed lines, with the $(\sqrt{3}\times\sqrt{3})$ R30° superstructure denoted as T, and the honeycomb superstructure as H, so as to readily identify the adjacent distribution of the $(\sqrt{3}\times\sqrt{3})$ R30° and honeycomb superstructures (see Fig. S2 in the Supporting Information for details). The zoomed-in STM topographic image clearly resolves the two kinds of superstructure, as shown in Fig. 1(b). The H_1 region manifests the original graphene lattice, while exhibiting a $(\sqrt{3}\times\sqrt{3})$ R30° and honeycomb superstructure at each side, denoted as T and H_2, respectively. A line profile measured along an atomic row reveals the height transition of the equivalent atom,

Supported by the National Natural Science Foundation of China (Grant Nos. 11674136 and 61901200), Yunnan Province for Recruiting High-Caliber Technological Talents (Grant No. 1097816002), Reserve Talents for Yunnan Young and Middle Aged Academic and Technical Leaders (Grant No. 2017HB010), the Yunnan Province Science and Technology Plan Project (Grant No. 2019FD041), the China Postdoctoral Science Foundation, and the Yunnan Province Postdoctoral Science Foundation.

*Corresponding author. Email: jclu@kust.edu.cn

© 2021 Chinese Physical Society and IOP Publishing Ltd

as marked by the yellow and white arrows in Fig. 1(c). In fact, the honeycomb superstructure has the same origin as the $(\sqrt{3}\times\sqrt{3})$ R30° superstructure, as shown by the corresponding model in Fig. 2(d). The honeycomb superstructure (yellow hexagon) occurs due to the overlap of two sets of intrinsic $(\sqrt{3}\times\sqrt{3})$ R30° superstructures (purple rhombuses) with a phase shift, resulting in an equivalent STM contrast of six atoms.

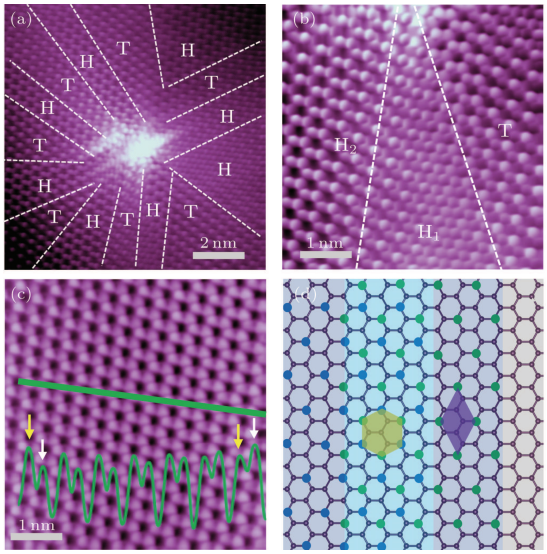

Fig. 1. Well-resolved superstructures around a defect on the HOPG surface: (a) Large-scale STM topography showing the defect in the center area with a high density of state. (b) Zoomed-in STM image of the superstructure area, with the honeycomb and $(\sqrt{3}\times\sqrt{3})$ R30° transition clearly distinguishable. (c) High resolution STM image of the superstructure: the inset shows the corresponding line profile measured along the green straight line. (d) The structural model of the $(\sqrt{3}\times\sqrt{3})$ R30° superstructure to honeycomb superstructure transition, the corresponding unit cells are denoted by a purple parallelogram and a dark yellow hexagon. Scanning parameters: (a) 10 mV, 500 pA; (b) 10 mV, 500 pA; and (c) 10 mV, 800 pA.

Previous studies of HOPG have identified wire-like structures with boundaries between misoriented grains in the crystalline structure. Those studies focused on the topographical features associated with GBs. Later theoretical and experimental work addressed questions regarding the electronic properties of GBs.[19–24] Attempts to grow wafer-size graphene by chemical vapor deposition (CVD) have revealed that the films are polycrystalline, consisting of micron-sized randomly oriented single crystal domains. The GBs between adjacent domains can be clearly observed via STM/S, whereas the connection between the morphology of a GB and its effect on the associated local spectrum is still a matter of debate. In our experiment, we investigated GBs of different widths and lengths. Interestingly, those GBs connecting differently oriented domains exhibit an amorphous feature, with only 2–4 repeating units. This is quite different from periodic GBs, as well as previously reported amorphous GB.[2,11,25] Figure 2(a) shows a quasi-periodic GB with a length of more than 40 nm, which disappears when reaching the step edge. The close-up STM image in Fig. 2(b) reveals the same superstructures discussed above, as indicated by the white arrows in Fig. 2(b). Compared to periodic GBs, the superstructure examined here has a far higher decay length. Owing to the amorphous features of the GB, it can be distinguished from as much as 10 nm away from the GB.

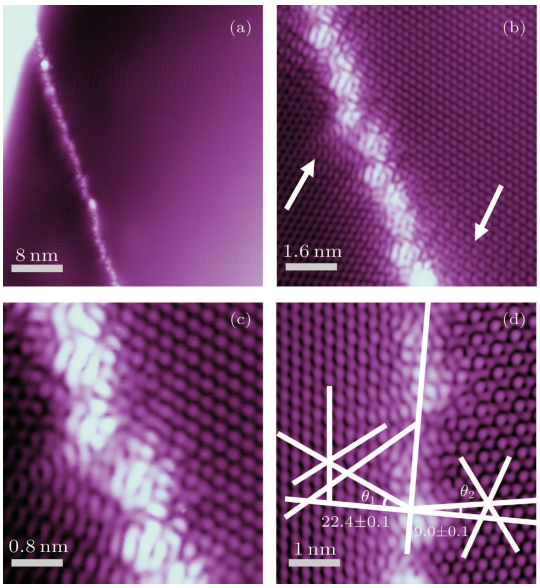

Fig. 2. STM topographies of the grain boundary on the HOPG surface: (a) Large-area STM image showing a 1D boundary as long as 40 nm connecting the upper and lower terraces. (b) Close-up STM image of the boundary, with superstructures denoted by white arrows. (c) and (d) High-resolution STM images of the boundary, with different atomic arrangements revealed at each side of the boundary, as marked in (d), where the angle between the equivalent atomic lines is 23.5°. Scanning parameters: (a) 200 mV, 100 pA, (b) 200 mV, 100 pA, (c) 200 mV, 100 pA, and (d) 60 mV, 300 pA.

To further characterize the detailed atomic structure of the GB segment on the HOPG surface, we attempted to measure the misorientation angle in the GB. In a regular GB, one can infer the misorientation angle between the grains, $\theta = \arcsin(b/2d)$, where d is the period of the pattern, and b is the length of the Burgers vector of the dislocation forming the GB. In the simplest possible situation, there is one dislocation per period, with the length of the Burgers vector, b, being equal to the lattice constant of graphene, where $a = 0.246$ nm. Thus, the period increases monotonically with decreasing misorientation angle. Despite the poor crystallinity, we can still deduce the misorientation angle of a specific segment via the following method: a vertical axis is drawn along the boundary, and the corresponding horizontal axis is perpendicular to it. The sums of the angle θ, corresponding to the grains to the left and right with respect to the

horizontal axis, are θ_1 and θ_2, respectively.[25] Figure 3(d) shows that the angle θ is close to 33.4°, where $\theta_1 \approx 22.4°$ and $\theta_2 \approx 9.0°$, taking the inaccuracy into consideration. It is reasonable to assign this GB segment to the 5- and 7-membered ring reconstruction, in accordance with the previous studies.[2,9,11]

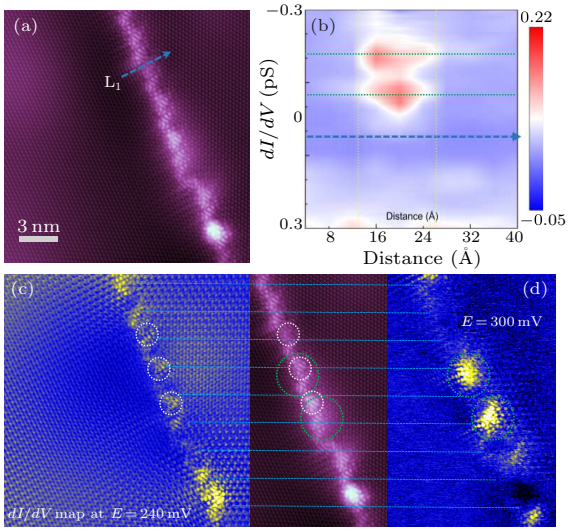

Fig. 3. STS measurements of the 1D grain boundary: (a) STM topography of the GB. (b) dI/dV line mapping, taken across the boundary, with a length of ∼40 Å, denoted with a blue dashed line, labeled as L_1 in (a). The states below the Fermi level occur exactly in the same region with the GB, as indicated by the two yellow dashed lines in (a) and (b). The emerging localized states are indicated by two green dashed lines. (c) and (d) dI/dV maps taken at energies of 240 mV and 300 mV. The two localized states in this segment are denoted by white and green circles, respectively. Scanning parameters: (a) 30 mV, 300 pA, (c) 240 mV, 300 pA, and (d) 300 mV, 300 pA.

GBs are known to accumulate or redistribute local charges, as the result of interlayer interactions, which may alter the electronic structure.[2,11,25,26] In Fig. 3(b), dI/dV curves taken across the GB revealed higher LDOS than the bulk region. Owing to the crystallinity, the LDOS is highly site-dependent. As denoted by the yellow dashed line in Fig. 3(b), dI/dV spectroscopy taken at line L_1 marked in Fig. 3(a) reveals higher LDOS, with a length of ∼18 Å, consistent with the lateral extent of the GB. In addition to the peaks detected here, at other sites, peaks at ∼240 mV and ∼300 mV emerge (see the Supporting Information for more details). To further examine the spatial distribution of these states, we conducted dI/dV mapping at a bias voltage of ∼240 mV and ∼300 mV, as displayed in Figs. 3(c) and 3(d). The state distributions exhibit the same spatial phase as the STM topographic periodicity, and are marked by green and white circles, respectively, providing more evidence of the repeated unit of this GB segment. To our surprise, the state at ∼300 mV seems to be more influenced by the GB segment bonding to it than the state at ∼240 mV, as the triple units exhibit the same states at ∼240 mV, while less evident states are distributed in the dI/dV mapping of energy of ∼300 mV.

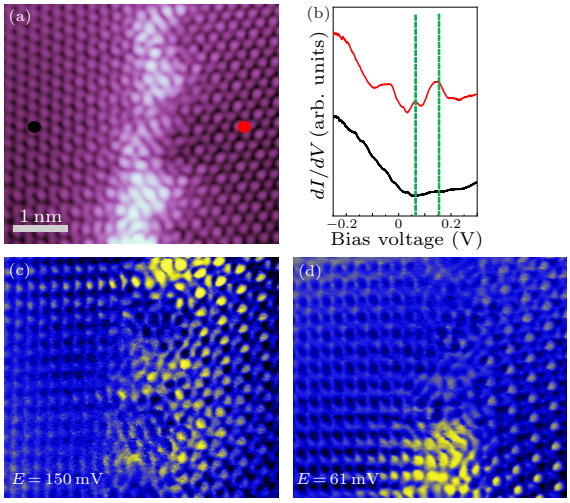

Fig. 4. STS measurements of the superstructure induced by GB: (a) atomic resolved STM image of the boundary area. (b) dI/dV taken at the positions marked by black and red dots in (a). (c) and (d) Corresponding dI/dV maps taken at the energy states indicated by the green dashed lines in (b). Scanning parameters: (a) 150 mV, 300 pA, (c) 150 mV, and (d) 61 mV.

In addition to the LDOS at GBs, we also carried out STS analysis at superstructures near the GB, as shown in Fig. 4(b), where the positions corresponding to each dI/dV curve are marked with black and red dots in Fig. 4(a). At the normal HOPG lattice, the dI/dV curve is featureless,[10,27–29] whereas at the superstructure region, the curve shows three main peaks at bias voltages of −40 mV, 61 mV and 150 mV, respectively. Two energy positions are selected to map the state distributions, as shown in Figs. 4(c) and 4(d). At each energy, the state distributes on the superstructure side as well as in parts of the GBs. We note that in previous reports,[11] the superstructure gives rise to an LDOS peak at ∼0.12 eV above the Fermi level, which is different from our results. To obtain a clearer understanding of the GB scattering, we analyzed the quantum quasi-particle interference (QPI) pattern (Fig. S4) using a fast Fourier transform (FFT) STS map of Fig. 4(d). The outermost green circles in Fig. S4b denote the surface graphene lattice. The intervalley scattering-related vectors are marked as red circles, and directly originate from the superstructures, as resolved via STM topographies [Fig. 4(a)]. Moreover, the intravalley scattering-related central bright region, as denoted by white circles in Fig. S4b, can also be resolved.[30] In addition to those mentioned above, two further pronounced scattering vectors can also be found in the FFT-STS map, as marked by yellow circles in Fig. S4b, implying additional electron scattering near the GB.[30–37] Furthermore, the states distribute over a wide area, which is also different from the previously recorded periodic or amorphous

GBs,[38] indicating the occurrence of stronger electron scattering near GBs. The decay length can be extracted via an FFT of the STM topographies. The oscillation amplitude of a specific scattering can be mapped using a line profile in an inverse FFT (see Fig. S5 for further detail) and is estimated to be 2.40 and 2.60 nm for the selected scattering patterns, which are longer than those formerly reported.[2,19,21,25,39,40] To the best of our knowledge, the electron wave scattering features probed by STM depend on the extent to which the defect influences the local electronic band structure, and the interactions between existing topological defects. In non-periodic GBs, the electronic modulation is highly site-dependent, giving different scattering potentials.[22,30,33–37] It has also been reported that interlayer coupling may enhance intervalley scattering in stacked double-layer graphene.[38] Further research is required to achieve a better understanding of these scattering behaviors.

In conclusion, we have investigated the electronic states induced by topological defects on HOPG surface, which manifested as $(\sqrt{3} \times \sqrt{3})$ R30° superstructures in STM topographies. In the vicinity of a point-like defect, the overlap of two sets of intrinsic $(\sqrt{3} \times \sqrt{3})$ R30° superstructures gives rise to a honeycomb superstructure. With reference to quasi-periodic GBs, in addition to localized states, we have also found electronic modulations of the HOPG lattice extending over several nanometers, indicating enhanced scattering behavior. These results may promote a deeper understanding of the physical and electronic structure of polycrystalline graphene, and contribute to the optimization of growth and fabrication protocols to control the effects of topological defects on its electrical transport properties.

References

[1] Ziatdinov M, Fujii S, Kusakabe K *et al.* 2013 *Phys. Rev. B* **87** 115427
[2] Yang B, Xu H, Lu J *et al.* 2014 *J. Am. Chem. Soc.* **136** 12041
[3] Xu W Y, Zhang L Z, Huang L *et al.* 2019 *Chin. Phys. B* **28** 046801
[4] Wu L, Hou T, Li Y *et al.* 2013 *J. Phys. Chem. C* **117** 17066
[5] Vicarelli L, Heerema S J, Dekker C *et al.* 2015 *ACS Nano* **9** 3428
[6] Hollen S M, Tjung S J, Mattioli K R *et al.* 2016 *J. Phys.: Condens. Matter* **28** 034003
[7] Banhart F, Kotakoski J and Krasheninnikov A V 2011 *ACS Nano* **5** 26
[8] Rehman M U, Hua C and Lu Y 2020 *Chin. Phys. B* **29** 057304
[9] Simonis P, Goffaux C, Thiry P A *et al.* 2002 *Surf. Sci.* **511** 319
[10] Sakai K I, Takai K, Fukui K I *et al.* 2010 *Phys. Rev. B* **81** 235417
[11] Luican-Mayer A, Barrios-Vargas J E, Falkenberg J T *et al.* 2016 *2D Mater.* **3** 031005
[12] Long F, Yasaei P, Sanoj R *et al.* 2016 *ACS Appl. Mater. & Interfaces* **8** 18360
[13] Li S Y, Ren Y N, Liu Y W *et al.* 2019 *2D Mater.* **6** 031005
[14] Li J, Lin L, Rui D *et al.* 2017 *ACS Nano* **11** 4641
[15] Kotakoski J, Krasheninnikov A V, Kaiser U *et al.* 2011 *Phys. Rev. Lett.* **106** 105505
[16] Sun Z P, Hua C Q, Liu X L *et al.* 2020 *Phys. Rev. B* **101** 155114
[17] Zhang W, Ju Z and Wu W 2019 *Phys. Rev. B* **100** 115120
[18] Ugeda M M, Brihuega I, Hiebel F *et al.* 2012 *Phys. Rev. B* **85** 121402
[19] Cervenka J and Flipse C F J 2009 *Phys. Rev. B* **79** 195429
[20] Cervenka J, Katsnelson M I and Flipse C F J 2009 *Nat. Phys.* **5** 840
[21] Gargiulo F and Yazyev O V 2014 *Nano Lett.* **14** 250
[22] Gunlycke D and White C T 2011 *Phys. Rev. Lett.* **106** 136806
[23] Lahiri J, Lin Y, Bozkurt P *et al.* 2010 *Nat. Nanotechnol.* **5** 326
[24] Meyer J C, Kisielowski C, Erni R *et al.* 2008 *Nano Lett.* **8** 3582
[25] Yazyev O V and Louie S G 2010 *Phys. Rev. B* **81** 195420
[26] Park J, He G, Feenstra R M *et al.* 2013 *Nano Lett.* **13** 3269
[27] López J C M, Passeggi M C G and Ferrón J 2008 *Surf. Sci.* **602** 671
[28] Niimi Y, Matsui T, Kambara H *et al.* 2006 *Phys. Rev. B* **73** 085421
[29] Ziatdinov M, Fujii S, Kusakabe K *et al.* 2014 *Phys. Rev. B* **89** 155405
[30] Rutter G M, Crain J N, Guisinger N P *et al.* 2007 *Science* **317** 219
[31] Yan H, Liu C C, Bai K K *et al.* 2013 *Appl. Phys. Lett.* **103** 143120
[32] Liu H, Chen J, Yu H *et al.* 2015 *Nat. Commun.* **6** 8180
[33] Iqbal M Z, Kelekci O, Iqbal M W *et al.* 2014 *New J. Phys.* **16** 083020
[34] Jung M, Sohn S D, Park J *et al.* 2016 *Sci. Rep.* **6** 22570
[35] Mahmood A, Mallet P and Veuillen J Y 2012 *Nanotechnology* **23** 055706
[36] Mallet P, Brihuega I, Bose S *et al.* 2012 *Phys. Rev. B* **86** 045444
[37] Tesch J, Leicht P, Blumenschein F *et al.* 2017 *Phys. Rev. B* **95** 075429
[38] Koepke J C, Wood J D, Estrada D *et al.* 2013 *ACS Nano* **7** 75
[39] Yang H, Mayne A J, Boucherit M *et al.* 2010 *Nano Lett.* **10** 943
[40] Wahl P, Schneider M A, Diekhoner L *et al.* 2003 *Phys. Rev. Lett.* **91** 106802

Supporting Information: Topological-Defect-Induced Superstructures on Graphite Surface

Zi-lin Ruan(阮子林), Zhen-liang Hao(郝振亮), Hui Zhang(张辉), Shi-jie Sun(孙诗杰), Yong Zhang(张永), Wei Xiong(熊玮), Xing-yue Wang(王兴悦), Jian-chen Lu(卢建臣)*, and Jin-ming Cai(蔡金明)

Faculty of Materials Science and Engineering, Kunming University of Science and Technology, Kunming 650000, China

* Supported by the National Natural Science Foundation of China (11674136, 61901200), the Thousand Talents Plan-The Recruitment Program for Young Professionals (1097816002), Yunnan Province for Recruiting High-Caliber Technological Talents (1097816002), reserve talents for Yunnan young and middle aged academic and technical leaders (2017HB010), the Yunnan Province Science and Technology Plan Project (Grant No. 2019FD041), the China Postdoctoral Science Foundation and the Yunnan Province Postdoctoral Science Foundation..

*Corresponding author. Email: jclu@kust.edu.cn.

1. Experimental details

All STM/S experiments were performed by using an ultrahigh vacuum low-temperature scanning tunneling microscopy (LT-STM) system (Scienta Omicron) with a base pressure better than 1×10^{-10} mbar. Fresh HOPG surface is cleaved using adhesive tape at atmosphere and transferred into load lock chamber immediately to avoid impurity adsorption. After degassed at 400°C overnight, the sample is transfer to STM. All STM/S measurements were performed at 4.2 K with a Pt/Ir tip, all topographic images were acquired in constant-current mode. For STS characterization, the dI/dV measurements have been performed with a lock-in amplifier (Zurich Instrument) that modulates the voltage bias at a frequency f = 599 Hz with an amplitude of ~20 mV.

2. STM topographies of typical defects on graphite surface.

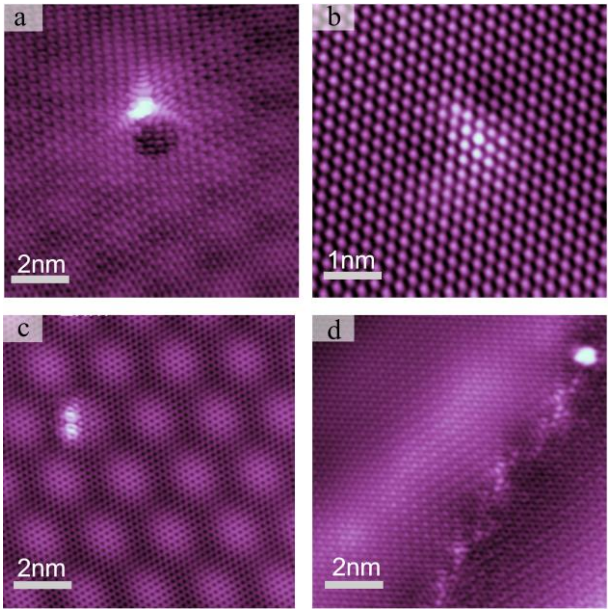

Figure S1. STM topographies of typical defects in natural graphite. a) single vacancy, b) heteroatom replacement. c, d) heterocycle located in a moiré region and grain boundary, pentagon-heptagon and pentagon-octagon defects are usually found in newly cleaved HOPG surface or grown graphene with low crystallinity. Scanning parameters: a)100 mV, 900 pA; b) 30 mV, 100 pA; c) 100 mV, 300 pA; and d) 200 mV, 10 pA.

3. Superstructure domain discrimination.

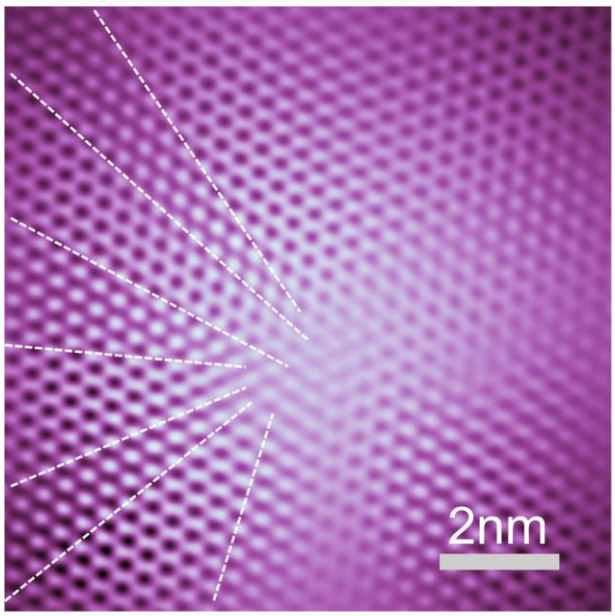

Figure S2. FFT filtered image of figure 1a, the honeycomb and single bright atom can be easily distinguished, corresponding to the honeycomb and $(\sqrt{3} \times \sqrt{3})$ R30 °superstructure, respectively.

4. Additional STS measured along the GB.

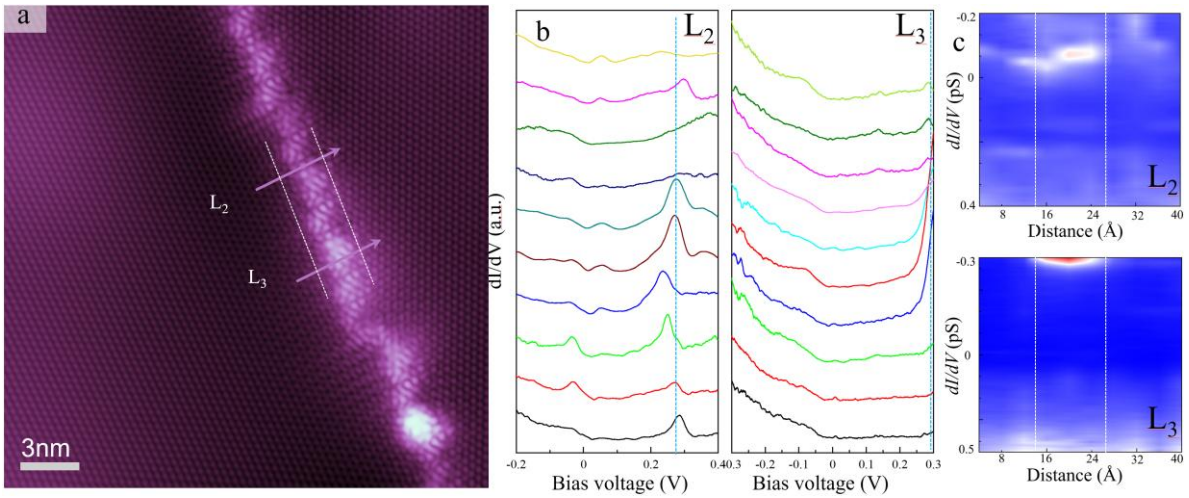

Figure S3. a) dI/dV curves taken across the boundary labeled as L2 and L3, the corresponding line mappings are show in figure c. Localized electronic states emerge at ~0.24 V and 0.3 V, as marked by light blue dashed line in b, the states have the same spatial distribution with the length of the GB.

5. Electron wave scattering behavior caused by the GB.

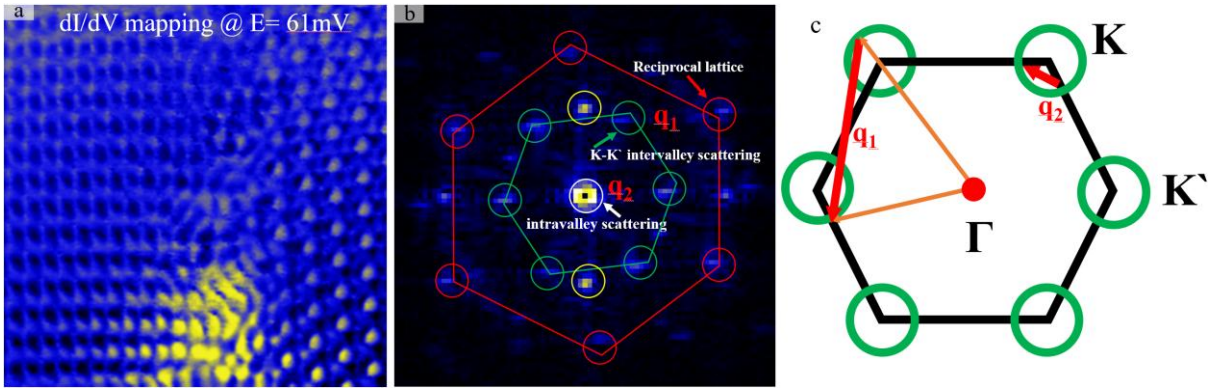

Figure S4. a) dI/dV mapping at 61 mV. b) FFT-STS map of figure a, the spot marked by red circles arise from surface graphene lattice, the intervalley scattering related spots are denoted with green circles, the center bright region indicates the intravalley related scatterings. Possible scattering channels are denoted by yellow circles in FFT-STS. c) Schematic of the 2D Brillouin zone (black lines), constant energy contours (green rings) at the K-K` points, and the two dominant classes of scattering vectors that create the interference patterns.

6. Decay length extraction.

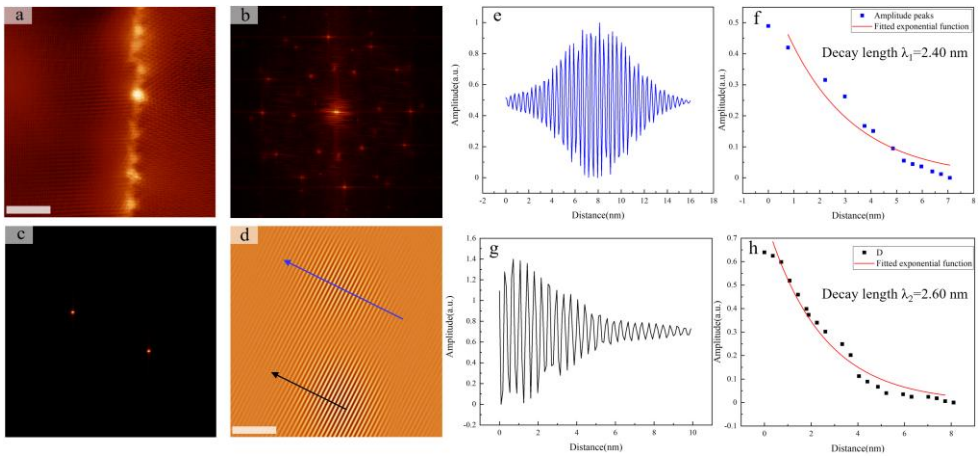

Figure S5. a, b) STM topography of GB and the corresponding Fast Fourier transform (FFT) pattern. c,d) two picked spot and its inversed real space pattern. Two line across the scattering pattern are indicated in d) with their line profiles showing in e and g, the interference propagates into the bulk with decreasing intensity and clear long-range oscillations in e and g. f, h)The corresponding peak intensities and fitted exponential decay function of e and g, giving decay length of 2.40 and 2.60 nm of selected scattering channel. Scale bar: 4 nm.